Journal of Metals, Materials and Minerals, 35(3), e2310, 2025

Macro-encapsulation of polyethylene glycol and magnetite (Fe_3O_4) in concrete as phase change materials for building thermal management

Muhammad FAUZI[1], Budhy KURNIAWAN[1,*], Anggito Pringgo TETUKO[2], Timbangen SEMBIRING[3], Fanna NILAM[3], Amdy FACHREDZY[1], and Perdamean SEBAYANG[2]

[1] *Department of Physics, Faculty of Mathematics and Natural Sciences, Universitas Indonesia, Jl. Prof. Dr. Mahar Mardjono-Depok, 16424, Indonesia*

[2] *Research Center for Advanced Materials, National Research and Innovation Agency (BRIN), Bld. 440, KST. B. J. Habibie-Tangerang Selatan, 15314, Indonesia*

[3] *Department of Physics, Faculty of Mathematics and Natural Sciences, Universitas Sumatera Utara, Jl. Bioteknologi No. 1-Medan, 20155, Indonesia*

***Corresponding author e-mail**: budhy.kurniawan@sci.ui.ac.id

Received date:
13 February 2025
Revised date:
13 May 2025
Accepted date:
20 May 2025

Keywords:
Phase change material;
Polyethylene glycol;
Fe_3O_4;
Macroencapsulation;
Thermal management

Abstract

Thermal management technology is a crucial strategy for reducing energy consumption in buildings by utilizing stored solar energy. This study developed a polyethylene glycol (PEG)-based phase-change material (PCM), selected for its superior physicochemical stability, high latent enthalpy, and environmental compatibility. To enhance thermal conductivity, 20 vol% magnetite (Fe_3O_4) was incorporated into the PEG matrix. The composite was synthesized via an ultrasonic-assisted method (37 kHz, 80°C, 1 h). X-ray diffraction (XRD) confirmed the crystalline structure of PEG and the cubic phase of Fe_3O_4, while Fourier-transform infrared spectroscopy (FTIR) validated the synthesis by identifying Fe–O, C–H, and O–H functional groups. Scanning electron microscopy (SEM) revealed a homogeneous dispersion of Fe_3O_4, and energy-dispersive X-ray spectroscopy (EDS) confirmed the elemental composition of C, H, O, and Fe. Vibrating sample magnetometry (VSM) demonstrated superparamagnetic behavior, with a saturation magnetization of 16.76 emu·g^{-1}. Thermal analysis indicated a 49% increase in thermal conductivity, a latent heat of 78.88 J·g^{-1}, and a melting temperature of 61.51°C. These findings underscore the potential of Fe_3O_4-enhanced PEG-based PCMs for efficient thermal regulation in buildings, contributing to enhanced energy efficiency and sustainability.

1. Introduction

An increase in high-temperature weather has become prevalent in recent years owing to global warming, particularly in the Middle East, Africa, and Asia [1]. This phenomenon has resulted in a surge in the demand for air conditioning in numerous regions, leading to increased energy consumption, carbon emissions, and environmental degradation. Recent studies have reported that energy use in buildings, on average, accounts for 40% of the total global energy consumption [2]. Consequently, there is a need for thermal regulations in buildings to reduce air conditioning usage, address the energy crisis, and mitigate global warming. One approach involves the use of thermal energy storage and thermal management systems for buildings. This technique can be implemented by utilising phase-change materials (PCMs) that undergo phase transitions at specific temperatures and absorb or release substantial amounts of latent heat [3]. PCMs are widely applied in solar energy storage systems, energy efficiency in buildings, thermal insulation and conditioning, and residual heat recycling to improve energy efficiency utilisation, owing to their advantages of good thermal stability, maintenance of nearly constant temperature during the phase transition process, and high chemical stability [4]. For instance, Hu *et al.*, 2024 [2] applied PCMs to regulate building temperatures in summer. TiO_2@n-octadecane, as the PCMs, exhibited a melting enthalpy of 120 J·g^{-1}. Subsequently, 20% TiO_2@n-octadecane microcapsules integrated in 5 mm concrete-maintained temperatures below 28.5°C for 15.7 min, 14.0 min, and 7.6 min at 30°C, 35°C, and 40°C, respectively. Additionally, Tetuko *et al.*, 2023 [5] analysed paraffin-magnetite composite PCMs inside concrete (50 mm × 50 mm × 50 mm) for thermal energy storage. The authors proposed that the heat transfer process could be efficiently received by PCMs inside concrete owing to its latent heat of 156.53 J·g^{-1}.

Phase change materials (PCMs) are categorised into organic, inorganic, and eutectic types based on their chemical composition [6]. Numerous studies have demonstrated the effectiveness of PCMs in regulating building temperatures, particularly organic-based ones. These organic PCMs offer advantages, such as high latent heat, greater enthalpy of vaporisation, cost-effectiveness, and compatibility with various metal containers [7]. Nevertheless, PCMs have drawbacks, including poor thermal conductivity (0.2 W·mK^{-1}), phase change leakage, low electrical conductivity for heat-to-electricity conversion, and weak solar energy absorption [8-10]. Jannah *et al.*, 2023 [11] explored PCMs with PEG4000-SiO_2 enhanced by Fe_3O_4-Graphene,

revealing that Fe_3O_4-Graphene influenced the crystal growth of Fe_3O_4-Graphene/PEG4000-SiO_2. The study found that increasing the Fe_3O_4-Graphene content in Fe_3O_4-Graphene/PEG4000-SiO_2 nanocomposites reduced the latent heat, although it remained above 100 $J \cdot g^{-1}$, indicating its suitability for heat storage [11]. Additionally, He *et al.*, 2022 examined the impact of adding 1 wt% and 3 wt% Fe_3O_4 to paraffin in composite PCMs, which resulted in improved thermal conductivity of 0.30 $W \cdot mK^{-1}$ and 0.34 $W \cdot mK^{-1}$, respectively [12].

In this study, composite phase-change materials (PCMs) were created from PEG 6000 with 20 vol% magnetite (Fe_3O_4) extracted from iron sand in West Java, Indonesia. The first novelty of the research is the high percentage (20%) of magnetite (Fe_3O_4) addition in PEG 6000 to enhance the thermal conductivity and melting rate of PCMs. The second novelty of this investigation focuses on the novel design of the macro-encapsulation tube embedded in the concrete. The uniquely designed encapsulation tube for storing PCMs aims to enhance heat transfer within concrete to act as a thermal management medium. The investigation encompassed analyses of the crystal structure, morphology, chemical bonding, magnetite characteristics, and thermal properties. The PEG6000@Fe_3O_4 based PCMs exhibited remarkable thermal stability and reliability. Given their straightforward synthesis process and comprehensive property analysis, these PCMs show promise for use as thermal regulators in building applications.

2. Materials and methodology

2.1 Materials

The PCMs were prepared using polyethylene glycol (PEG 6000) acquired from Sigma-Aldrich in the form of white granules with a molar mass of 6000 $g \cdot mol^{-1}$ and a melting temperature of 56°C to 53°C. Fe_3O_4 was obtained from an iron sand synthesis process in West Java, Indonesia. In addition, cement, sand, aggregate, water, and copper tubes were employed as materials for the fabrication of concrete as a medium for macroencapsulating PCMs.

2.2 Preparation of PCMs

The PCMs composites were prepared following a two-step process, as illustrated in Figure 1. PEG6000, which served as the PCMs matrix, was initially melted at 80°C using an ultrasonic bath to facilitate the dispersion of Fe_3O_4 particles. Subsequently, 20 vol% Fe_3O_4 particles were incorporated into the fully melted PEG 6000. The temperature was maintained constant and a power frequency of 37 kHz was utilised for the homogenisation process between PEG 6000 and Fe_3O_4. This process was performed for 1 h with manual stirring to ensure material homogenisation stability. Following the homogenisation of the composite PCMs material, the samples were moulded for characterisation testing and macroencapsulation stability testing on concrete.

2.3 Preparation macroencapsulation in concrete

Macroencapsulation of PCMs was conducted by incorporating PCMs into concrete that had been combined with copper tubes. The concrete was fabricated using cement, sand, aggregate, and water in a ratio of 2:3:4:1.4, with concrete moulds measuring 5 cm × 5 cm × 5 cm.

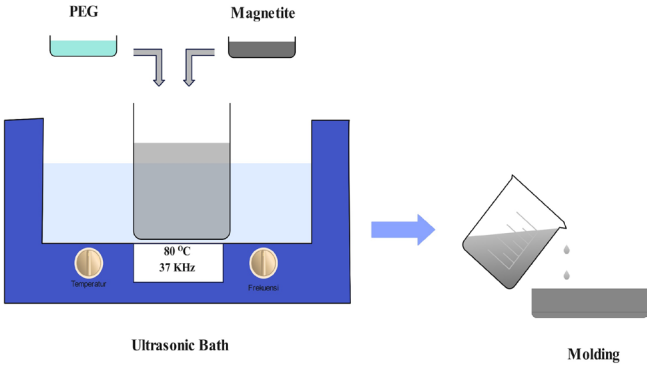

Figure 1. Process of PCMs composite synthesis.

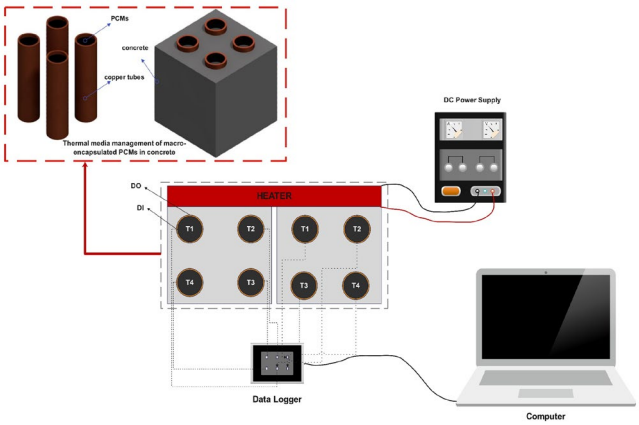

Figure 2. Schematic of PCMs thermal management testing in concrete.

Copper tubes (diameter: 1.25 cm; length: 5 cm) arranged in a four-square configuration were embedded into the concrete matrix. The concrete composition ratio, as identified by Donza *et al.* [13] demonstrates significant compressive strength and is well suited for the manufacturing process when combined with copper tubing. The PCM used in this study was a composite of polyethylene glycol (PEG) as the base material, with 20 vol% Fe_3O_4 nanoparticles as a thermal conductivity enhancer. This PCM composite was filled into the copper tubes prior to the concrete curing process. Subsequently, the concrete curing process was performed for 28 days at ambient temperature (24°C to 27°C). Following the completion of the concrete production process, the synthesized PCMs were introduced into the concrete in their liquid form. This step facilitated the macro-encapsulation process and established the density of the PCMs within the copper tube. Consequently, concrete with macro-encapsulated PCMs was prepared for thermal testing, which is intended to improve the building's thermal management. The macro-design of PCM encapsulation in concrete is shown in Figure 2.

2.4 Characterization and instruments

In this study, physical and thermal analyses were performed. The crystalline phases of the Fe_3O_4 and PEG 6000 particles were analysed by X-ray Diffraction (XRD) (Rigaku). Additionally, chemical structure was assessed via Fourier transform infrared spectroscopy (FTIR). Morphological analysis was performed using Scanning electron microscopy with Energy dispersive X-ray spectroscopy (SEM-EDS) (Jeol JSM-IT200). Magnetic properties were characterised using

a Vibrating sample magnetometer (VSM). Furthermore, thermal analysis of the PCMs was carried out using a thermal conductivity test (type: QTM-500), Differential scanning calorimetry (DSC), and a macro-encapsulated thermal distribution test system with devices, as illustrated in Figure 2. K-type thermocouples were connected to an Arduino-based digital readout monitor. Thermal distribution measurements were conducted over a 24 h period daily. Temperature distribution experiments were performed to evaluate the thermal performance of the PCMs encapsulated in concrete.

3. Results and discussions

3.1 Crystal structure analysis of PEG 6000 and Fe_3O_4

The crystal structure dynamics of the PEG 6000 and Fe_3O_4 particles were analysed using X-ray diffraction (XRD). Figure 3 shows the XRD patterns of both the PEG 6000 and Fe_3O_4 particles. The diffraction spectra of PEG 6000 Figure 3(a) confirm its polymeric salam crystallinity, with prominent peaks at 19.29° and 23.41° (2θ), aligning with Et-tanteny *et al.*, 2024 [14]. Conversely, the XRD pattern of Fe_3O_4 particles Figure 3(b) reveals crystal peaks at 18.26°, 30.03°, 35.37°, 37.00°, 42.99°, 53.33°, 56.85°, 62.43°, and 73.48° (2θ), corresponding to the (111), (022), (113), (222), (400), (422), (333), (044), and (335) planes per the COD database: 96-900-9769, indicating a cubic crystal structure. These findings are consistent with Liu *et al.*, 2024 [15].

The crystal sizes and structural parameters of the Fe_3O_4 particles were measured using Rietveld refinement data, the refinement process is conducted with fullprof software with a pseudo voigt approach. Furthermore, the results of the refinement of the experimental Fe_3O_4 XRD pattern with the database obtained the chi2 value: 2.62. The rietveld refinement pattern is shown in Figure 4(a) and the WH plot is in Figure 4(b). Crystallite size was determined via the Scherrer Equation and Williamson-Hall (WH) plot [16]:

$$D = \frac{K\lambda}{\beta\cos\theta} \quad (1)$$

$$\beta\cos\theta = \frac{K\lambda}{D} + 4\varepsilon\sin\theta \quad (2)$$

Where β is the full width at half maximum (FWHM), λ is the wavelength of X-ray, D is the crystallite size, θ is the Bragg angle, and k is the Scherrer constant (0.94). The WH plot method also estimates microstrain (ε), indicating nanoparticle lattice strain [15]. Fe_3O_4 particle crystallite sizes were 27.81 nm (Scherrer Equation) and 30.81 nm (WH), exceeding those reported by Antarnusa *et al.*, 2022 [17]. The results of the additional parameter analyses are presented in Table 1.

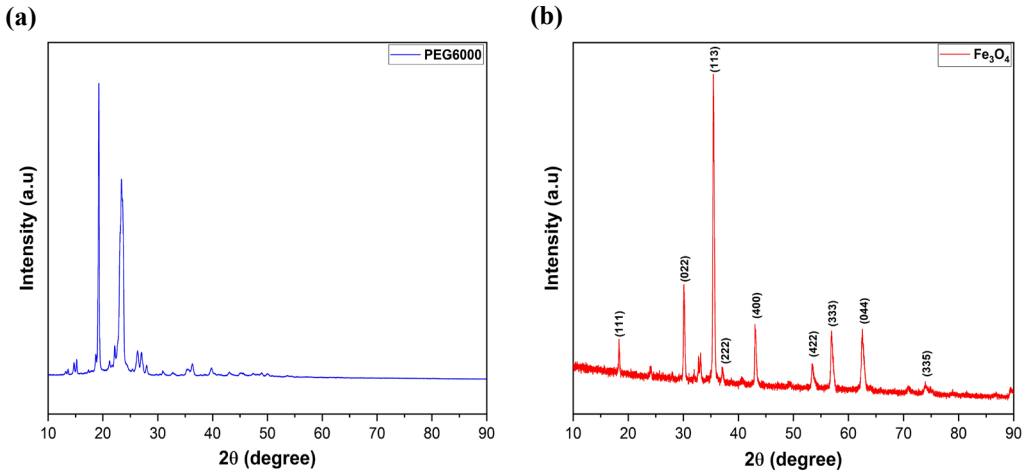

Figure 3. XRD peak pattern results (a) PEG 6000, and (b) Fe_3O_4.

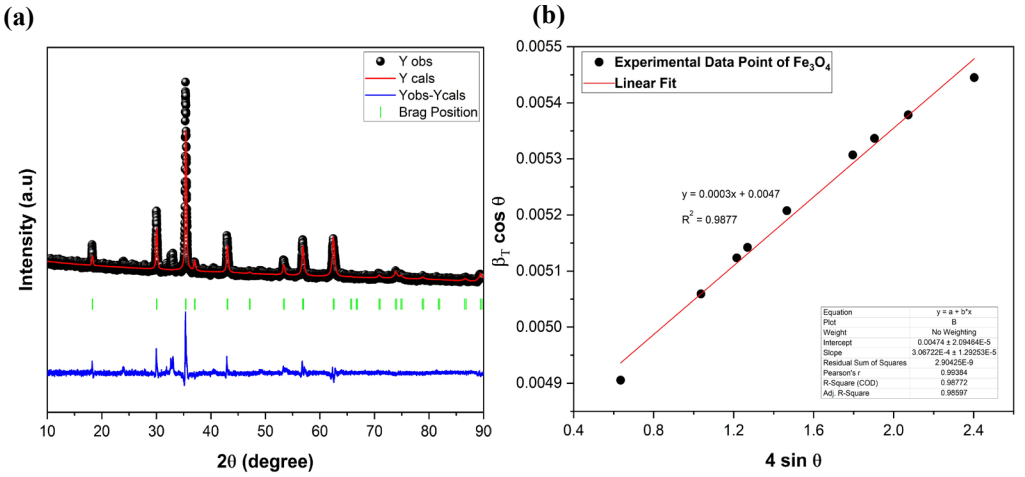

Figure 4. (a) Rietveld refinement analysis of Fe_3O_4, and (b) Plot obtained from williamson-hall method of Fe_3O_4.

Table 1. Crystal structure parameters of Fe_3O_4.

Parameters	Unit	Fe_3O_4
Space Group	-	Fd-3m
a	Å	8.407
b	Å	8.407
c	Å	8.407
V	$Å^3$	594.329
Crystallite size Scherrer	nm	27.81
Crystallite size WH	nm	30.81
ε	%	0.0003

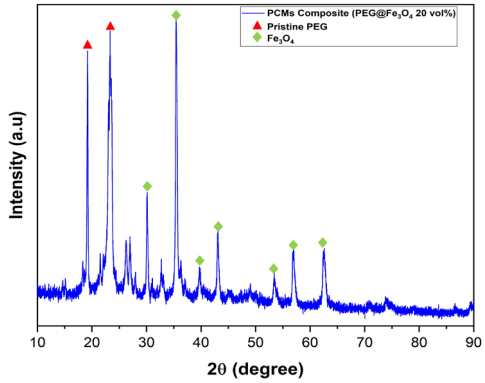

Figure 5. XRD peak pattern results of PCMs Composite (PEG 6000@Fe_3O_4 20 vol%).

Furthermore, Figure 5 shows the XRD patterns of the PCMs composite samples. The absence of new peaks suggests that a composite consisting of pristine PEG 6000 and Fe_3O_4 magnetite was successfully synthesized. This result is consistent with the previous findings [18,19]. The Fe_3O_4 particles were dispersed throughout the PEG 6000 layers, and their interactions remained purely physical with no evidence of chemical reactions occurring between the components [19].

3.2 Chemical structure analysis of PCMs

Fourier-transform infrared (FTIR) spectroscopy analysis confirmed the chemical structure of the PEG 6000-based composite phase change materials (PCMs) incorporated with 20 vol% Fe_3O_4 as illustrated in Figure 6. The characteristic peak of Fe_3O_4, shown in Figure 6(a), appears at a wavelength of 531 cm^{-1}, corresponding to the stretching vibration of the Fe–O bond [20]. This finding is consistent with the results reported by Khoshnam and Salimijazi, [21] who identified Fe_3O_4 vibrations within the range of 474 cm^{-1} to 570 cm^{-1}. Similarly, Astuti *et al.* [22] observed Fe–O tetrahedral and Fe–O octahedral bond vibrations at wave numbers of 545.86 cm^{-1} and 484.14 cm^{-1}, respectively.

Figure 6(b) presents the FTIR spectrum of the PEG 6000–Fe_3O_4 composite PCM. A distinct peak at 3450 cm^{-1} corresponds to the O–H stretching vibrations, characteristic of PEG's hydrophilic nature and water solubility [23]. The C–H bonds in PEG are evident at 1343 cm^{-1} and within the range of 1100 cm^{-1} to 1280 cm^{-1}, associated with symmetric and asymmetric C–O–C stretching vibrations, respectively [24]. Additionally, peaks observed at 963 cm^{-1} and 842 cm^{-1} are indicative of C=C bonds, while the absorption band at 1647 cm^{-1} is attributed to C=O stretching vibrations [25]. A weak absorption peak at 2866 cm^{-1} corresponds to C–H stretching vibrations [17]. Notably, a minor peak at 531 cm^{-1} also attributed to the Fe–O vibration further confirms the presence of Fe_3O_4 in the composite. The absence of new absorption peaks indicates that the interaction between PEG 6000 and Fe_3O_4 is physical in nature, rather than chemical. This confirms the successful synthesis of the PEG 6000–Fe_3O_4 composite PCMs without the formation of new chemical bonds.

3.3 Morphology of PCMs

Surface morphological analysis of the PCMs was conducted using SEM at 12 keV. As shown in Figure 7, Fe_3O_4 particles appear as bright regions and are generally distributed across the PEG 6000 matrix with irregular particle shapes. However, some areas exhibited visible clustering of Fe_3O_4 particles. This aggregation can be attributed to the intrinsic magnetic nature of Fe_3O_4, where magnetic dipole–dipole interactions and van der Waals forces promote particle attraction and clustering [11]. Additionally, suboptimal dispersion during the synthesis process particularly insufficient mixing time may contribute to localized agglomeration [26]. Although some degree of particle aggregation was observed, the use of a relatively high Fe_3O_4 concentration (20 vol%) is intentionally employed to significantly enhance the thermal conductivity of the PCM. Higher concentrations of thermally conductive fillers are known to facilitate the formation of continuous heat conduction pathways, which are essential for improving thermal response rates. While uniform dispersion is ideal, a controlled trade-off between filler concentration and aggregation is sometimes necessary to achieve notable performance gains. The observed improvements in thermal conductivity and phase-change response in this study suggest that the benefits of higher Fe_3O_4 loading outweigh the potential drawbacks from minor particle aggregation. Furthermore, as illustrated in the histogram of particle size distribution, a mean value of 0.45 μm was observed, this result exceeds those of previous studies and is attributable to the synthesis of magnetic Fe_3O_4 from natural iron sand [12,18,27]. On the other hand, the elemental analysis report through EDS revealed that the elements C, O, and Fe were present at 46.34 wt%, 26.43 wt% and 27.23 wt% or 64.33 at%, 27.54 at% and 8.13 at% respectively. These results closely align with the composition of the PCMs, where the addition of Fe_3O_4 was 20 vol%. This finding corroborates the investigation of Karaagac and Kockar [20], which confirmed the morphological results of Fe_3O_4 particles distributed in a diffuse manner with an irregular Fe_3O_4 particle shape.

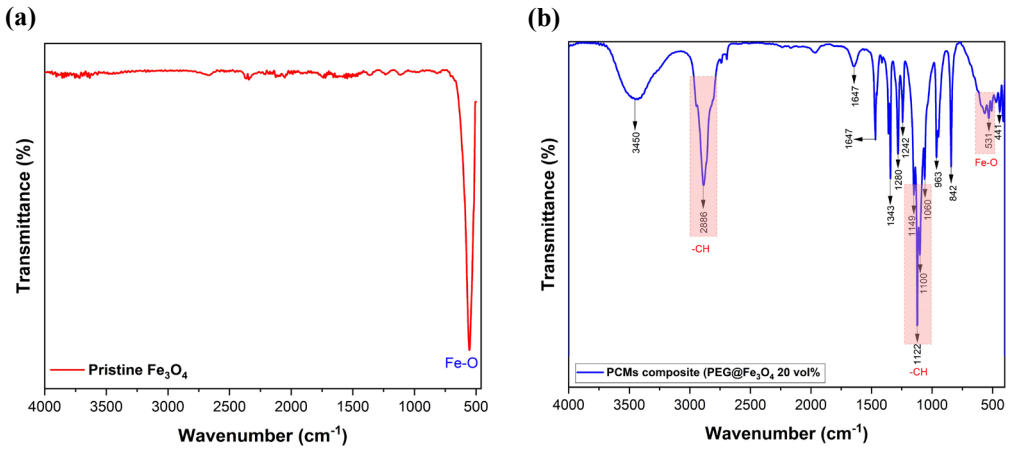

Figure 6. (a) FTIR spectra of pristine Fe_3O_4, and (b) FTIR spectra of the PEG 6000-Fe_3O_4.

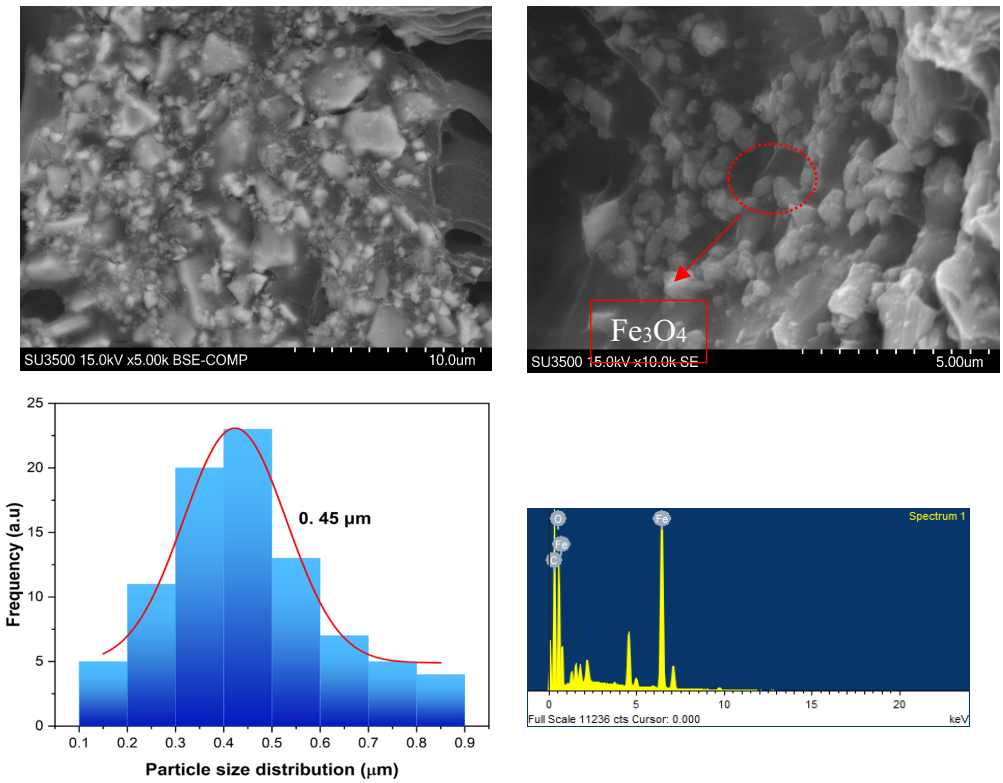

Figure 7. PCMs composite morphology, particle size distribution, and EDS analysis.

3.4 Magnetic properties analysis of PCMs

The magnetic characteristics of the PEG6000- Fe_3O_4 PCMs samples were evaluated using a VSM at ambient temperature. Figure 8(a) demonstrates that the synthesised sample exhibits superparamagnetic behaviour, with a coercivity of 169.22 Oe, corresponding to the remanent magnetisation (the residual magnetisation after the magnetic field is removed) [28]. The coercivity field on the hysteresis curve represents the strength of the magnetic field required to reduce the remanent magnetisation to zero at room temperature [29]. Furthermore, the sample is categorised as soft magnetic owing to the narrow area and symmetrical reverse order of the hysteresis curve when subjected to an external magnetic field [30]. The shape of the curve indicates that small particles have a strong magnetic response. This phenomenon occurs because smaller grain sizes in magnetic nanoparticles lead to unstable magnetic moments, as the anisotropic energy of magnetic nanoparticles is low [31]. Consequently, when exposed to an external magnetic field, the magnetic moment in small nanoparticles responds more rapidly. Subsequently, the magnetic property parameters were determined from the hysteresis curves by fitting them using the type-2 Langevin equation (Equation (3)), as illustrated in Figure 8(b) [32].

$$M = M_s \left[coth \left(\frac{\mu H}{k_B T} \right) - \frac{\mu H}{k_B T} \right] + \chi H + M_r \qquad (3)$$

The magnetic properties of PEG600-Fe_3O_4 yielded a maximum saturation magnetisation (M_S) of 16.76 emu·g^{-1} with an applied external magnetic field of ±20 kOe and a remanence of 2.76 emu·g^{-1}. This value is lower than the pristine Fe_3O_4 measurement of 77.26 emu·g^{-1}

in earlier research by Antarnusa *et al.* [33]. This reduction can be attributed to the size and shape of the magnetic nanoparticles (Fe_3O_4), which influences the physical properties that affect the magnetic response. The magnetic properties of the material are also influenced by the extent of particle size distribution, as the domain structure and magnetisation process are size-dependent. Moreover, the adsorption of nonmagnetic PEG molecules onto the magnetite particle surface may contribute to the decreased magnetisation value of PEG6000-Fe_3O_4.

3.5 Thermal conductivity of PCMs

The thermal conductivity of PCMs was analysed to investigate the increase in the efficiency of PCMs for thermal management in buildings. A higher thermal conductivity results in a more rapid thermal transfer process, thereby improving the performance of PCMs thermal management systems in buildings. In this study, the thermal conductivity of PEG6000-Fe_3O_4 20 vol% was determined to be 0.31 $W{\cdot}mK^{-1}$, which, when compared with pristine PEG, represented an increase of 49% [34]. The observed enhancement in thermal conductivity due to the incorporation of 20 vol% Fe_3O_4 plays a critical role in improving the performance of PEG6000-based PCMs for thermal regulation applications. Higher thermal conductivity facilitates a faster phonon transfer rate within the material, which accelerates the heat exchange process and shortens the phase transition duration [35-38]. This means that the PCM can absorb and release thermal energy more quickly and efficiently during heating and cooling cycles. In practical terms, this behavior enhances the responsiveness of the thermal storage system in real-world applications, such as maintaining indoor temperature stability in buildings. Moreover, although a slight reduction in latent heat was observed, the improved thermal response time can outweigh this trade-off, especially in dynamic thermal environments where rapid heat regulation is more beneficial than maximum energy storage. Thus, the synergistic effect of enhanced thermal conductivity and stable phase-change behavior positions PEG6000@Fe_3O_4 PCMs as promising candidates for passive thermal management in energy-efficient building materials. The percentage increase in thermal conductivity was calculated using Equation (4) [39].

$$\text{Percentage of enhancement} = \left(\frac{K_{PCMs} - K_{PEG}}{K_{PCMs}}\right) \times 100 \qquad (4)$$

Where K_{PCMs} represents the thermal conductivity of PEG6000-Fe_3O_4, and K_{PEG} represents the conductivity of pristine PEG 6000. Furthermore, in comparison with PEG@magnetite 50 wt% [5] and PEG@MWCNTs 1 wt% [34], significant differences were observed, with results of 0.53 $W{\cdot}mK^{-1}$ and 0.37 $W{\cdot}mK^{-1}$, respectively. This disparity was attributed to the variation in the quantity of particle additives incorporated into PEG 6000 and the nature of the particles. Additionally, the non-linear fluctuations in thermal conductivity are a consequence of the non-uniform distribution of particles in the PEG [40].

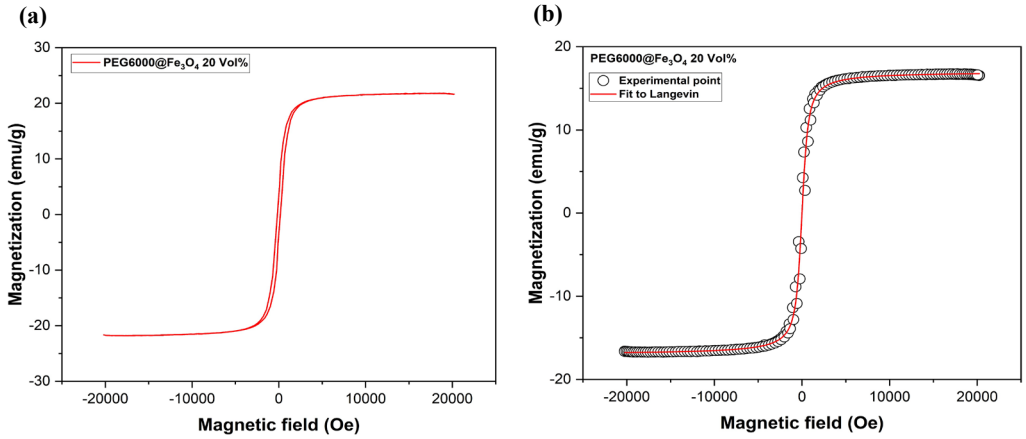

Figure 8. (a) Hysteresis curve of Fe_3O_4, and (b) Fitting hysteresis curve with langevin equation.

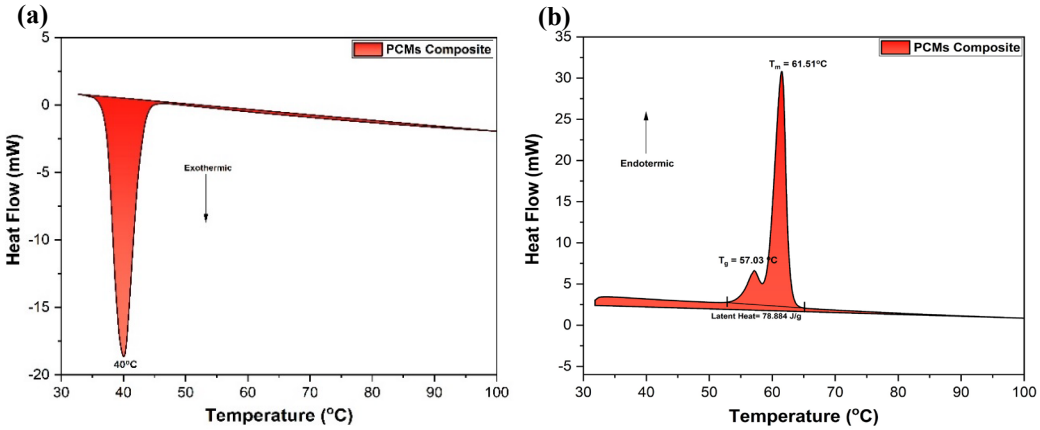

Figure 9. Solid-liquid phase transition DSC analysis graph, (a) Exothermic, and (b) Endothermic

3.6 Thermal stability of PCMs

The thermal stability performance of the investigated PCMs is presented in Figure 9, and the latent heat enthalpy and latent heat enthalpy efficiency are listed in Table 2. The efficiency is calculated using Equation (5) [41].

$$E = \left(\frac{\Delta H_m(PCM_S)}{\Delta H_m(PEG)}\right) \times 100\% \quad (5)$$

Where *E* represents the enthalpy efficiency, ΔHm (PCMs) denotes the enthalpy of melting of the composite PCMs, and ΔHm (PEG) denotes the enthalpy of melting of PEG.

As presented in Table 2, the PCMs in this study exhibited a latent heat of 78.88 $J \cdot g^{-1}$. This result indicates that the efficiency level of adding 20 vol% Fe_3O_4 to PEG6000 compared to PEG 6000 is 44.16% [26]. This finding suggests that the range remains within parameters suitable for thermal management applications. The decrease in latent heat observed in PEG6000- Fe_3O_4 occurs because of the increased thermal conductivity, resulting in a more rapid heat absorption (endothermic) process and, consequently, lower heat storage compared to pristine PEG6000. Conversely, the study by Cheng *et al.*, 2024 [42] confirmed that the addition of PEG-TiO_2 resulted in a significant decrease in latent heat enthalpy, attributed to the brief heat transfer process caused by increased thermal conductivity agglomeration. Furthermore, the variation in latent heat can be attributed to the incorporation of additives into the PCM composites, which enhances the thermal conductivity of the PCMs. Consequently, the phase change process requires less energy [43-45]. In addition, Figure 9(a) demonstrates that during the endothermic process or solid-to-liquid phase change, the PCMs exhibit a characteristic glass transition temperature at 57.03°C, indicating the polymeric nature of the PCMs material [39]. The peak melting temperature of the PCMs occurs at 61.51°C, which is lower than that of pristine PEG6000 and PEG600-SiO_2. During the exothermic heat release process (exothermic), the peak temperature of the solidification process occurred at 40°C.

3.7 Performance thermal analysis of macroencapsulation PCMs in concrete

A custom-built system featuring a heater at 80°C was used to evaluate the thermal management capabilities of the composite PCMs in concrete. The experiment involved six points for temperature distribution analysis, as illustrated in Figure 2. During heat transfer, the composite PCMs encapsulated in concrete generally absorb thermal energy. The temperature-time curve exhibited an inflection point at the PCMs' melting point, indicating the onset of phase change and thermal energy storage with minimal temperature fluctuation, as shown in Figure 10. Upon deactivation of the heat source, the temperature of the sample decreased until it reached the crystallisation point [50]. Subsequently, the temperature-time curve displayed an inflection point as the PCM solidified. Once the phase-change process was concluded, the curve resumed a steep downward trajectory.

In comparison, the PEG6000-Fe_3O_4 time-temperature curve at point T5 Do exhibited the highest temperature among all test points, absorbing up to 59.36°C due to its proximity to the heat source. Points T1 and T6 Di followed with similar temperature readings, differing only in their positions relative to the concrete PCMs (T1 inside, T6 Di outside). The subsequent analysis points were T2, T4, and T3, with maximum heat absorption temperatures of 57.84°C, 55.08°C, and 53.89°C, respectively. This thermal distribution analysis demonstrates that PCMs encapsulated in concrete can effectively receive and absorb thermal energy, rendering them suitable for thermal regulation in buildings [51-53], as shown in Figure 11. The graphical behaviour observed in this study aligns with research conducted by *Tetuko et al.*, 2023 [5], Li *et al*., 2023 [54], and Zahir *et al*., 2021 [1].

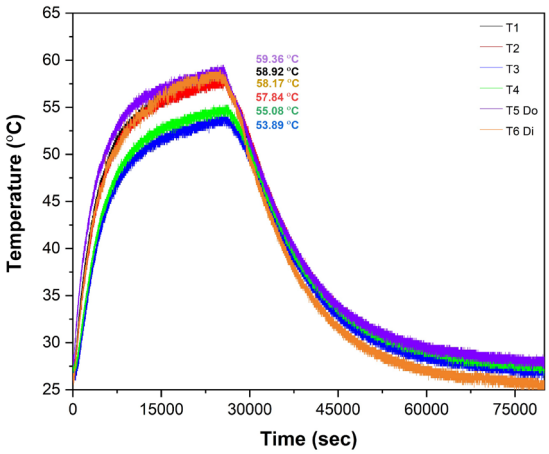

Figure 10. Time vs temperature graph of thermal distribution analysis of PCMs in concrete.

Table 2. Comparison of DSC characterisation results with previous research.

PCMs	Ts [°C]	Tm [°C]	ΔHs [$J \cdot g^{-1}$]	ΔHm [$J \cdot g^{-1}$]	ΔTs [$J \cdot g^{-1}$]	E [%]	Reference
PEG6000	35.3	61.7	167.1	178.6	24.3	-	[26]
PEG6000-Fe_3O_4	40	61.51	-	78.88	21.5	44.16	This work
PEG6000-CaO_4Si	44.1	57	106.8	122.1	12.9	55.17	[46]
PEG6000-SiO_2	37.9	61.7	160.1	164.9	23.8	92.32	[26]
PEG-diatomite	-	59.5	-	111.3	-	62.31	[46]
PEG-MWCNTs-1	37.24	56.45	123.14	125.9	-	-	[47]
PEG-MWCNTs-2	35.50	61.75	167.87	175.91	-	-	[47]
PEG-TiO_2	31	55.1	113.1	128.3	24.1	-	[48]
PEG-UMSNOs-0.5 wt%	41.83	60.89	145.49	157.05	19.06	-	[49]

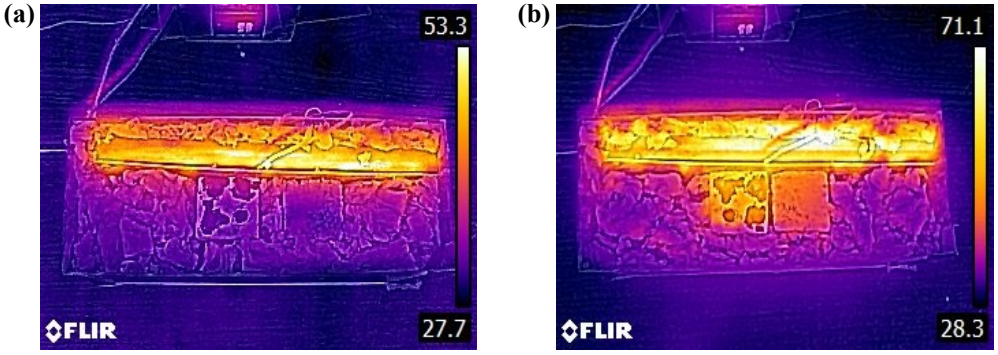

Figure 11. Thermal camera results of thermal distribution test of PCMs in concrete, (a) Endothermic, and (b) Thermal storage.

4. Conclusion

In this study, PEG 6000-based PCMs were successfully enhanced in terms of their thermal-physical properties through the dispersion of Fe_3O_4 particles. An ultrasonic method was employed in this experimental study, wherein PCMs were utilised as a regulatory mechanism for controlling heat in building systems. The results of physical analysis via XRD characterisation demonstrated that PEG 6000 is a crystalline polymer and Fe_3O_4 is a cubic crystal, with the crystal size calculated using the Debye-Scherrer Equation and Williamson-Hall plot of 27.81 nm and 30.81 nm. The successful synthesis of PCMs composites was confirmed by FTIR and VSM results, which indicated that the functional groups of the chemical compounds consisted of C–H–O and Fe–O bonds. Furthermore, the PCM composites exhibited superparamagnetic properties, which are characteristic of Fe_3O_4. Additionally, the thermal characteristics revealed an increase in the thermal conductivity of the PCMs by 49% compared to that of pristine PEG 6000. Differential scanning calorimetry (DSC) results also confirmed that the latent heat of the PCMs at 78.88 $J \cdot g^{-1}$ remains within appropriate limits. Moreover, the results of thermal distribution tests on PCMs-encapsulated concrete demonstrated that PCMs are capable of absorbing the applied heat, with the highest endothermic temperature reaching 59.36°C. The thermal conductivity improvement of the PCMs and the novel design of the encapsulation tube in the concrete enhance the heat transfer and can be applied as a thermal management medium.

Credit authorship contribution statement

Muhammad Fauzi: Writing – original draft, Methodology, Formal analysis, Data Curation, Project administration. **Budhy Kurniawan**: Supervision, Funding acquisition, Conceptualization, Validation. **Anggito Pringgo Tetuko**: Supervision, Writing – review & editing, Resources. Conceptualization. **Timbangen Sembiring**: Validation. **Fanna Nilam**: Investigation. **Amdy Fachredzy**: Experimental setup. **Perdamean Sebayang**: Validation.

Acknowledgements

The authors gratefully acknowledge the Research Center for Advanced Materials, National Research and Innovation Agency (BRIN), Indonesia for providing the necessary facilities. Furthermore, the authors express their gratitude to BRIN for awarding Muhammad Fauzi the Degree by Research Scholarship, designated by "NOMOR 27/II/HK/2024", Penelitian Dasar Unggulan Perguruan Tinggi 2024 "NKB-677/UN2.RST/HKP.05.00/2024" and JSPS Core-to-Core Program (JPJSCCB20240005)."

References

[1] Md. H. Zahir, M. M. Rahman, S. K. S. Basamad, K. O. Mohaisen, K. Irshad, M. M. Rahman, Md. A. Aziz, A. Ali, and M. M. Hossain, "Preparation of a sustainable shape-stabilized phase change material for thermal energy storage based on Mg^{2+}-doped $CaCO_3$/PEG composites," *Nanomaterials*, vol. 11, p. 1639, 2021.

[2] T. Hu, J. Zhang, R. Xiao, G. Wang, W. Yu, H. Su, and L. Su, "Study on the preparation and properties of TiO_2@n-octadecane phase change microcapsules for regulating building temperature," *Applied Thermal Engineering*, vol. 249, p. 123429, 2024.

[3] Y. Liu, L. Sun, J. Zheng, L. Yang, L. Jiang, and Y. Song, "Numerical simulation study of the phase transition heat transfer of nanoparticle-enhanced heat storage tubes," *Applied Thermal Engineering*, vol. 231, p. 121010, 2023.

[4] P. K. S. Rathore, and S. K. Shukla, "Enhanced thermophysical properties of organic PCM through shape stabilization for thermal energy storage in buildings: A state of the art review," *Energy Build*, vol. 236, p. 110799, 2021.

[5] A. P. Tetuko, A. M. S. Sebayang, A. Fachredzy, E. A. Setiadi, N. S. Asri, A. Y. Sari, F. Purnomo, C. Muslih, M. A. Fajrin, and P. Sebayang, "Encapsulation of paraffin-magnetite, paraffin, and polyethylene glycol in concretes as thermal energy storage," *Journal of Energy Storage*, vol. 68, p. 107684, 2023.

[6] P. K. S. Rathore, N. K. Gupta, D. Yadav, S. K. Shukla, and S. Kaul, "Thermal performance of the building envelope integrated with phase change material for thermal energy storage: An updated review," *Sustainable Cities and Society*, vol. 79, p. 103690, 2022.

[7] H. Togun, H. S. Sultan, H. I. Mohammed, A. M. Sadeq, N. Biswas, H. A. Hasan, R. Z. Homod, A. H. Abdulkadhim, Z. M. Yaseen, and P. Talebizadehsardari, "A critical review on phase change materials (PCM) based heat exchanger: Different hybrid techniques for the enhancement," *Journal of Energy Storage*, vol. 79, p. 109840, 2024.

[8] W. Wang, M. M. Umair, J. Qiu, X. Fan, Z. Cui, Y. Yao, and B. Tang, "Electromagnetic and solar energy conversion and

storage based on Fe_3O_4-functionalised graphene/phase change material nanocomposites," *Energy Convers Manag*, vol. 196, pp. 1299-1305, 2019.

[9] J. Yang, L.-S. Tang, L. Bai, R.-Y. Bao, Z.-Y. Liu, B.-H. Xie, M.-B. Yang, and W. Yang, "High-performance composite phase change materials for energy conversion based on macroscopically three-dimensional structural materials," *Mater Horiz*, vol. 6, pp. 250-273, 2019.

[10] W. Aftab, X. Huang, W. Wu, Z. Liang, A. Mahmood, and R. Zou, "Nanoconfined phase change materials for thermal energy applications," *Energy & Environmental Science*, vol. 11, pp. 1392-1424, 2018.

[11] W. N. Jannah, A. Taufiq, S. Zulaikah, A. Hidayat, E. Suharyadi, S. T. Wicaksono, and S. Sunaryono, "Fe_3O_4-graphene/polyethylene glycol-SiO_2 as a phase change material for thermal energy storage," *Materials Chemistry and Physics*, vol. 310, p. 128457, 2023.

[12] W. He, Y. Zhuang, Y. Chen, and C. Wang, "Experimental and numerical investigations on the melting behavior of Fe_3O_4 nanoparticles composited paraffin wax in a cubic cavity under a magnetic-field," *International Journal of Thermal Sciences*, vol. 184, p. 107961, 2023.

[13] H. Donza, O. Cabrera, and E. F. Irassar, "High-strength concrete with different fine aggregate, *Cement and Concrete Research*, vol. 32, no. 11, pp. 1755-1761, 2002.

[14] R. Et-tanteny, B. El Amrani, I. Manssouri, and H. Limami, "Physicochemical, mechanical and thermal analysis of unfired clay bricks: Kaolinite-PEG 6000 composite," *Cleaner Engineering and Technology*" vol. 22, p. 100793, 2024.

[15] C. Liu, L. Wang, Y. Li, X. Diao, C. Dong, A. Li, and X. Chen, "Fe_3O_4/carbon-decorated graphene boosts photothermal conversion and storage of phase change materials," *Journal of Colloid and Interface Science*" vol. 657, p. 590-597, 2024.

[16] A. C. B. Jesus, J. R. Jesus, R. J. S. Lima, K. O. Moura, J. M. A. Almeida, J. G. S. Duque, and C. T. Meneses, "Synthesis and magnetic interaction on concentrated Fe_3O_4 nanoparticles obtained by the co-precipitation and hydrothermal chemical methods," *Ceramics International*, vol. 46, p. 11149-11153, 2020.

[17] G. Antarnusa, P. D. Jayanti, Y. R. Denny, and A. Suherman, "Utilization of co-precipitation method on synthesis of Fe_3O_4/PEG with different concentrations of PEG for biosensor applications," *Materialia (Oxf)*, vol. 25, p. 101525, 2022.

[18] B. Lu, Y. Zhang, J. Zhang, J. Zhu, H. Zhao, and Z. Wang, "Preparation, optimization and thermal characterization of paraffin/nano-Fe_3O_4 composite phase change material for solar thermal energy storage, *Journal of Energy Storage*, vol. 46 p. 103928, 2022.

[19] Y. Hu, L. Shi, Z. Zhang, Y. He, and J. Zhu, "Magnetic regulating the phase change process of Fe_3O_4-paraffin wax nanocomposites in a square cavity," *Energy Conversion and Management*, vol. 213, p. 112829, 2020.

[20] O. Karaagac, and H. Köçkar, "Improvement of the saturation magnetization of PEG coated superparamagnetic iron oxide nanoparticles," *Journal of Magnetism and Magnetic Materials*, vol. 551, p. 169140, 2022.

[21] M. Khoshnam, and H. Salimijazi, "Synthesis and characterization of magnetic-photocatalytic Fe_3O_4/SiO_2/a-Fe_2O_3 nano core-shell," *Surfaces and Interfaces*, vol. 26, p. 101322, 2021.

[22] Astuti, S. Arief, M. Muldarisnur, Zulhadjri, and S. R. A. Usna, "Enhancement in photoluminescence performance of carbon-based Fe_3O_4@ZnO–C nanocomposites," *Vacuum*, vol. 211, p. 111935, 2023.

[23] D.-L. Zhao, P. Teng, Y. Xu, Q.-S. Xia, and J.-T. Tang, "Magnetic and inductive heating properties of Fe_3O_4/polyethylene glycol composite nanoparticles with core–shell structure," *Journal of Alloys and Compounds*, vol. 502, pp. 392-395, 2010.

[24] S. C. Mohanta, A. Saha, and P. S. Devi, "PEGylated iron oxide nanoparticles for pH responsive drug delivery application," *Materials Today: Proceedings*, vol. 5, pp. 9715-9725, 2018.

[25] X. Wang, Y. Zhao, X. Jiang, L. Liu, X. Li, H. Li, and W. Liang, "In-situ self-assembly of plant polyphenol-coated Fe_3O_4 particles for oleaginous microalgae harvesting," *Journal of Environmental Management*, vol. 214, pp. 335-345, 2018.

[26] B. Li, D. Shu, R. Wang, L. Zhai, Y. Chai, Y. Lan, H. Cao,and C. Zou, "Polyethylene glycol/silica (PEG@SiO_2) composite inspired by the synthesis of mesoporous materials as shape-stabilized phase change material for energy storage," *ReNew Energy*, vol. 145, pp. 84-92, 2020.

[27] B. Lu, Y. Zhang, J. Zhang, J. Zhu, H. Zhao, and Z. Wang, "Preparation, optimization and thermal characterization of paraffin/nano-Fe_3O_4 composite phase change material for solar thermal energy storage," *Journal Energy Storage*, vol. 46, p. 103928, 2022.

[28] P. Liu, Z. Yao, V. M. H. Ng, J. Zhou, L. B. Kong, and K. Yue, "Facile synthesis of ultrasmall Fe_3O_4 nanoparticles on MXenes for high microwave absorption performance," *Composites Part A: Applied Science and Manufacturing*, vol. 115, pp. 371-382, 2018.

[29] M. Abboud, S. Youssef, J. Podlecki, R. Habchi, G. Germanos, and A. Foucaran, "Superparamagnetic Fe_3O_4 nanoparticles, synthesis and surface modification," *Materials Science in Semiconductor Processing*, vol. 39, pp. 641-648, 2015.

[30] E. A. Setiadi, P. Sebayang, M. Ginting, A. Y. Sari, C. Kurniawan, C. S. Saragih, and P. Simamora, "The synthesization of Fe_3O_4 magnetic nanoparticles based on natural iron sand by co-precipitation method for the used of the adsorption of Cu and Pb ions," *Journal of Physics: Conference Series*, vol. 776, p. 012020, 2016.

[31] M. A. Medina, G. Oza, A. Ángeles-Pascual, M. González M., R. Antaño-López, A. Vera, L. Leija, E. Reguera, L. G. Arriaga, J. M. Hernández Hernández, and J. T. Ramírez, "Synthesis, characterization and magnetic hyperthermia of monodispersed cobalt ferrite nanoparticles for cancer therapeutics," *Molecules*, vol. 25, p. 4428, 2020.

[32] J.-L. Huang, L.-Q. Fan, Y. Gu, C.-L. Geng, H. Luo, Y.-F. Huang, J.-M. Lin, and J.-H. Wu, "One-step solvothermal synthesis of high-capacity Fe_3O_4/reduced graphene oxide composite for use in Li-ion capacitor," *Journal of Alloys and Compounds*, vol. 788, pp. 1119-1126, 2019.

[33] G. Antarnusa, and E. Suharyadi, "A synthesis of polyethylene glycol (PEG)-coated magnetite Fe_3O_4 nanoparticles and their

characteristics for enhancement of biosensor," *Materials Research Express*, vol. 7, p. 056103, 2020.

[34] Y. Harmen, Y. Chhiti, F. E. M'Hamdi Alaoui, F. Bentiss, C. Jama, S. Duquesne, and M. Bensitel, "Thermal performance of PEG-MWCNTs composites as shape-stabilised phase change materials for thermal energy storage," *Fullerenes, Nanotubes and Carbon Nanostructures*, vol. 29, pp. 732-738, 2021.

[35] S. A. B. Al-Omari, Z. A. Qureshi, F. Mahmoud, and E. Elnajjar, "Thermal management characteristics of a counter-intuitive finned heat sink incorporating detached fins impregnated with a high thermal conductivity-low melting point PCM," *International Journal of Thermal Sciences*, vol. 175, p. 107396, 2022.

[36] M. A. Fikri, A. K. Pandey, M. Samykano, K. Kadirgama, M. George, R. Saidur, J. Selvaraj, N. A. Rahim, K. Sharma, and V. V. Tyagi, "Thermal conductivity, reliability, and stability assessment of phase change material (PCM) doped with functionalized multi-wall carbon nanotubes (FMWCNTs)," *Journal Energy Storage*, vol. 50, p. 104676, 2022.

[37] S. Wu, T. Yan, Z. Kuai, and W. Pan, "Thermal conductivity enhancement on phase change materials for thermal energy storage: A review," *Energy Storage Materials*, vol. 25, pp. 251-295, 2020.

[38] N. Şahan, M. Fois, and H. Paksoy, "Improving thermal conductivity phase change materials - A study of paraffin nano-magnetite composites," *Solar Energy Materials and Solar Cells*, vol. 137, pp. 61-67, 2015.

[39] R. Bharathiraja, T. Ramkumar, M. Selvakumar, and N. Radhika, "Thermal characteristics enhancement of Paraffin Wax Phase Change Material (PCM) for thermal storage applications," *ReNew Energy*, vol. 222, p. 119986, 2024.

[40] N. H. Mohamed, F. S. Soliman, H. El Maghraby, and Y. M. Moustfa, "Thermal conductivity enhancement of treated petroleum waxes, as phase change material, by α nano alumina: Energy storage," *Renewable and Sustainable Energy Reviews*, vol. 70, pp. 1052-1058, 2017.

[41] X. Li, X. Sheng, Y. Guo, X. Lu, H. Wu, Y. Chen, L. Zhang, and J. Gu, "Multifunctional HDPE/CNTs/PW composite phase change materials with excellent thermal and electrical conductivities," *Journal of Materials Science and Technology*, vol. 86, pp. 171-179, 2021.

[42] X. Cheng, Q. Feng, W. Ni, X. Li, Y. Qi, S. Zhang, Q. Wu, and Z. Huang, "Stable and reliable PEG/TiO_2 phase change composite with enhanced thermal conductivity based on a facile sol-gel method without deionized water," *Journal Energy Storage*, vol. 89, p. 111705, 2024.

[43] M. N. Sam, A. Caggiano, C. Mankel, and E. Koenders, "A comparative study on the thermal energy storage performance of bio-based and paraffin-based PCMs using DSC procedures," *Materials*, vol. 13, no. 13, p. 1705, 2020.

[44] B. K. Choure, T. Alam, and R. Kumar, "A review on heat transfer enhancement techniques for PCM based thermal energy storage system," *Journal Energy Storage*, vol. 72, p. 108161, 2023.

[45] P. K. S. Rathore, and S. K. Shukla, "An experimental evaluation of thermal behavior of the building envelope using macro-encapsulated PCM for energy savings," *ReNew Energy*, vol. 149, pp. 1300-1313, 2020.

[46] T. Qian, J. Li, X. Min, W. Guan, Y. Deng, and L. Ning, "Enhanced thermal conductivity of PEG/diatomite shape-stabilized phase change materials with Ag nanoparticles for thermal energy storage," *Journal of Materials Chemistry A*, vol. 3, no. 16, pp. 8526-8536, 2015.

[47] Y. Harmen, Y. Chhiti, F. E. M'Hamdi Alaoui, F. Bentiss, C. Jama, S. Duquesne, and M. Bensitel, "Thermal performance of PEG-MWCNTs composites as shape-stabilised phase change materials for thermal energy storage," *Fullerenes*, *Nanotubes and Carbon Nanostructures*, vol. 29, pp. 732-738, 2021.

[48] X. Cheng, Q. Feng, W. Ni, X. Li, Y. Qi, S. Zhang, Q. Wu, and Z. Huang, "Stable and reliable PEG/TiO_2 phase change composite with enhanced thermal conductivity based on a facile sol-gel method without deionized water," *Journal Energy Storage*, vol. 89, p. 111705, 2024.

[49] S. P. Chitriv, K. Dharmadhikari, A. Nithin, A. S. Archak, R. P. Vijayakumar, and G. C. DSouza, "Unzipped multiwalled carbon nanotube oxide/PEG based phase change composite for latent heat energy storage," *International Journal of Heat and Mass Transfer*, vol. 220, p. 124908, 2024.

[50] H. Jouhara, A. Żabnieńska-Góra, N. Khordehgah, D. Ahmad, and T. Lipinski, "Latent thermal energy storage technologies and applications: A review," *International Journal of Thermofluids*, vol. 5-6, p. 100039, 2020.

[51] S. Wu, T. Yan, Z. Kuai, and W. Pan, "Thermal conductivity enhancement on phase change materials for thermal energy storage: A review," *Energy Storage Materials*, vol. 25, pp. 251-295, 2020.

[52] Y. Lin, Y. Jia, G. Alva, and G. Fang, "Review on thermal conductivity enhancement, thermal properties and applications of phase change materials in thermal energy storage," *Renewable and Sustainable Energy Reviews*, vol. 82, pp. 2730-2742, 2018.

[53] G. Alva, Y. Lin, and G. Fang, "An overview of thermal energy storage systems," *Energy*, vol. 144, pp. 341-378, 2018.

[54] J. Li, Q. Chang, C. Xue, J. Yang, and S. Hu, "Carbon dots efficiently enhance photothermal conversion and storage of organic phase change materials through interfacial interaction," *Carbone New York*, vol. 203, pp. 21-28, 2023.